Title

Exercise history predicts focal differences in bone volume fraction, mineral density and microdamage in the proximal sesamoid bones of Thoroughbred racehorses

Journal

Journal of Orthopaedic Research®, 40(12)

ISSN

0736-0266

Authors

Shaffer, Sarah K

Garcia, Tanya C

Stover, Susan M

et al.

Publication Date

2022-12-01

DOI

10.1002/jor.25312

Received: 27 October 2021 | Revised: 27 January 2022 | Accepted: 1 March 2022

DOI: 10.1002/jor.25312

RESEARCH ARTICLE

Journal of Orthopaedic Research®

Exercise history predicts focal differences in bone volume fraction, mineral density and microdamage in the proximal sesamoid bones of Thoroughbred racehorses

Sarah K. Shaffer[1] | Tanya C. Garcia[2] | Susan M. Stover[2] | David P. Fyhrie[3,4]

[1]Department of Mechanical Engineering, University of California Davis, Davis, California, USA

[2]Department of Surgical and Radiological Sciences, School of Veterinary Medicine, University of California Davis, Davis, California, USA

[3]Department of Biomedical Engineering, University of California Davis, Davis, California, USA

[4]Department of Orthopaedic Surgery, University of California Davis, Davis, California, USA

Correspondence

Sarah K. Shaffer, Department of Mechanical Engineering, University of California, Davis, 1 Shields Avenue, Davis, CA 95616, USA.
Email: skshaffer@ucdavis.edu

Funding information

Center for Equine Health at University of California Davis; University of California, Davis (Maury Hull Fellowship); California Thoroughbred Foundation (Louis R. Rowan Fellowship); Grayson-Jockey Club Research Foundation

Abstract

Medial proximal sesamoid bones (PSBs) from Thoroughbred racehorses that did (Case) or did not (Control) experience unilateral biaxial PSB fracture were evaluated for bone volume fraction (BVF), apparent mineral density (AMD), tissue mineral density (TMD), and microdamage in Case fractured, Case contralateral limb intact, and Control bones. A majority of Case bones had a subchondral lesion with high microdamage density, and low BVF, AMD, and TMD. Lesion microdamage and densitometric measures were associated with training history by robust linear regression. Exercise intensity was negatively related to BVF ($0.07 \le R^2 \le 0.12$) and positively related to microcrack areal density ($0.21 \le R^2 \le 0.29$) in the lesion; however, in an undamaged site, the relationships were opposite in direction. Regardless of location, TMD decreased with event frequency for both Case and Control, suggesting increased bone remodeling with exercise. Measures of how often animals were removed from active training (layups) predicted a decrease in TMD, AMD, BVF, and microdamage at regions away from the lesion site. A steady-state compartment model was used to organize the differences in the correlations between variables within the data set. The overall conclusions are that at the osteopenic lesion site, repair of microdamage by remodeling was not successful (e.g., lower bone mass, increased damage, and lower mineralization) but that in regions away from the lesion remodeling successfully controlled damage (e.g., higher bone mass, less microdamage, and lower mineralization).

KEYWORDS

biomechanics, bone, injury prevention, modeling, racehorse

1 | INTRODUCTION

Proximal sesamoid bone (PSB) fracture is a common fatal injury among Thoroughbred racehorses.[1–3] A subchondral bone lesion has been observed in medial PSBs from both forelimbs of racehorses that sustain unilateral biaxial PSB fracture.[3–5] Bilateral bone lesions, consistent fracture configurations, and association with high-speed exercise support that PSB fractures are stress fractures.[4–7]

Stress fractures are similar to fatigue fractures of nonliving materials. However, unlike in nonliving materials, bone reacts to damage, mechanical loads, and environmental factors.[8–10] In healthy bone, cells modulate the quantity of bone and turnover rate in

response to the load environment and to repair damaged tissue.[11] Bone reacts to these stimuli through two processes: modeling and remodeling. During remodeling the cellular processes of bone resorption and formation are coupled, but they are uncoupled during modeling. Microdamaged tissue is removed and replaced with undamaged tissue by remodeling. The newly formed tissue mineralizes, with the time and rate of mineralization partially controlled by bone cells.[12] Resorption reduces the apparent elastic modulus by forming pores that can be stress risers at the site of damage repair.[13] Consequently, damage formation and porosity may increase at the repair site in a vicious cycle if training is not reduced.[1,6,9,14,15] In healthy adults, the amount of tissue removed and formed during remodeling are approximately the same (i.e., balanced). However, both negative (e.g., the formation of Haversian canals during remodeling of primary cortical bone) and positive (e.g., in cancellous bone a positive remodeling balance can be induced with parathyroid hormone)[16,17] remodeling balances are possible.

A compartment model for the "bone tissue turnover cycle" is proposed (Figure 1). It separates bone tissue into four volumes: undamaged mineralized bone (BV_{UD}), damaged mineralized bone (BV_D), osteoid (OV), and marrow or vascular space (MV). These tissue types are defined histologically[18] and completely fill the tissue volume ($TV = BV_D + BV_{UD} + MV + OV$). Tissue types can transform along designated paths at the corresponding rates (k_1–k_5; Figure 1 and Supporting Information C). The rates are known to vary with mechanical loading (e.g., strain frequency, magnitude, and so on), age, and other biological factors. Each compartment is a volumetric average within the TV. Volume averaging of tissue types is analogous to many morphometric measures, which define properties relative to a set referent (i.e., measure per volume).[18] The four tissue types are related to histological measures, including bone volume fraction (BVF) and void space (1 − BVF) as measured by microcomputed tomography (μCT). In this case, BVF is equivalent to the mineralized BVF (BV_M/TV, where $BV_M/TV \equiv (BV_D + BV_{UD})/TV$) and void space (1 − BVF) is equivalent to the unmineralized BVF (BV_{UM}/TV, where $BV_{UM}/TV \equiv (OV + MV)/TV$).

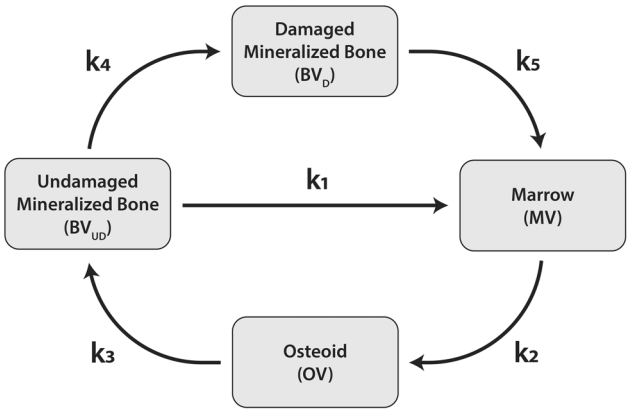

FIGURE 1 Compartment model of bone remodeling that assumes a volume of bone tissue can be classified into four distinct types: undamaged mineralized bone, damaged mineralized bone, osteoid, and marrow. The arrows indicate the path a volume subunit can follow to transform into the different tissue types and k_i are the transformation rates

The tissue turnover cycle (Figure 1) represents both bone modeling and remodeling. However, changes to any volume fraction cannot be directly attributed to either process. When bone is mathematically characterized using volume fractions, the internal surfaces are lost and, therefore, the distinction between bone remodeling and pure internal (i.e., trabecular [TB] surface) modeling is also lost. For example, an increase in mineralized BVF could occur by unbalanced positive remodeling, modeling to widen trabeculae, and/or other additive changes, but the model cannot distinguish the processes used to increase mineralized TV fraction. This model retains the concept of modeling on anatomical bone surfaces, as exterior surfaces remain after volume averaging. However, in the current study, we are only considering internal changes in tissue fractions below the joint surface; therefore, the model represents changes in volume fractions due to internal modeling and remodeling.

Objectives were to (1) compare densitometric and microdamage measures in the medial PSBs of racehorses that did (Case) and did not (Control) sustain unilateral biaxial PSB fracture, (2) determine relationships between measures and high-speed exercise, and (3) assess the model as a mechanism to understand the results.

2 | MATERIALS AND METHODS

Densitometric and microdamage parameters were measured in 10 fractured medial PSBs (FX-PSB) from Case racehorses killed due to unilateral biaxial PSB fracture (1 female, 5 castrated males, 4 males; 2–8 years old), 10 contralateral limb intact medial PSBs (CLI-PSBs) from the same Case racehorses, and 10 medial PSBs from Control racehorses (CTRL-PSBs) killed for injuries unrelated to PSB fracture (3 female, 5 castrated males, 2 males; 2–7 years old). The medial FX-PSBs had either a simple ($n = 8$) or comminuted ($n = 2$) transverse midbody fracture configuration. The lateral FX-PSBs were not examined, but sustained either a midbody or oblique fracture. Study horses were selected from a larger group of California racehorses that were killed due to musculoskeletal injuries, while in race-training from 2000 to 2017.[4] Horses were selected using an exercise-related stratified random sampling technique (see "Study 1" of Shaffer et al.[4]), so that a wide range of racehorse exercise histories would be represented. Specimens were collected at necropsy and stored until studied, as previously reported.[4] This study was exempt from Institutional Animal Care and Use Committee approval.

2.1 | Subject specific exercise history

The date and distance for all official lifetime racing-speed activities were acquired (Jockey Club Information Systems). Individual Events were classified as a Race (i.e., a competition) or Work (i.e., a training activity). Sixty-seven derived variables represented four categories:

lifetime exercise, exercise intensity, layup (≥60 days without an Event), and exercise intensity in the year before death (Table S-A1)[7].

2.2 | Specimen preparation

PSBs were imaged using μCT (μCT 35, ScanCo Medical; 18.5 μm^3 cubic voxels at 7 kVP, 114 μA, 2.5 s integration time) calibrated to a phantom and segmented at the same threshold. A global threshold of 540 mg HA/ccm was determined by examining candidate thresholds and choosing that which best segregated the tissue into solid and void at the TB level as determined by one observer (SKS).

PSBs were previously assessed for focal discoloration, presence of a radiolucent bone lesion, and sectioned into 3 mm-thick serial sagittal sections.[4] The section with the greatest focal subchondral discoloration was selected for microdamage measurement, as it correlated with lesion presence.[4] Similarly located sections were selected for PSBs without focal discoloration.

Sections were stored in 70% ethanol for 8 days then en bloc stained in 1% basic fuchsin (F98-10, Fischer Chemical) in ascending grades of ethanol (80%, 90%, 100%; 6 days/grade) under vacuum.[19–21] Stained samples were infused in glycol methacrylate resin (Technovit 7200, Exakt Technologies, Inc./Kulzer) in descending grades of ethanol (70%, 30%, 0%; 7 days/grade) under vacuum, placed in a mold, and cured for 8 h of white then blue light (Histolux, Exakt Technologies, Inc.). Hardened blocks were mounted (Technovit 4000 and 7210) on plastic slides, sectioned to 400 μm, then ground and polished to 70 μm thickness (Exakt 400 CS grinder, Exakt Apparateau GmH & Co.; Buehler MicroPolish 1 μm). Brightfield digital microscopy images (Olympus VS120; Olympus OlyVia) were manually stitched (Adobe Photoshop) for microdamage quantification.

2.3 | Densitometric assessment

BVF, apparent mineral density (AMD), and tissue mineral density (TMD) were quantified in four 166.5 μm-wide regions of interest (μROIs) on μCT reconstructions (Figure 2; ScanCo μCT Evaluation Software v6.5-3; ScanCo Medical) by one observer. In bones with a lesion, μROIs were created on the sagittal μCT slice with maximum lesion area. In PSBs without a lesion, the μROIs were created on the sagittal μCT slice at 34.5% of the axial–abaxial width from the most abaxial slice, the mean location of maximum lesion sagittal area in CLI-PSBs. The four μROIs were as follows: central subchondral (CS), central subchondral border (CSB), proximal subchondral (PS), and TB μROI (Figure 2).

2.4 | Microdamage quantification

Microdamage was quantified for six histology ROIs (hROIs) by one observer (SKS), blinded to group (CLI and CTRL, but not FX) and horse (ImageJ).[22] Three 1.5 mm-deep quadrilateral regions equally divided the articular surface and formed the PS, CS, and distal subchondral (DS) hROIs. The proximal deep (PD), central deep (CD), and distal deep (DD) hROIs were duplicated palmarly (Figure 2).

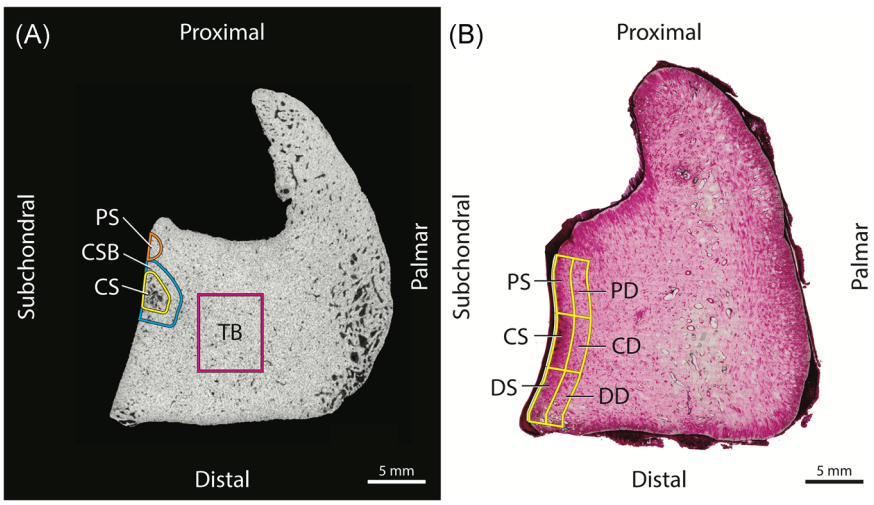

FIGURE 2 (A) Sagittal-plane microcomputed tomography (μCT) from a case contralateral intact (CLI) proximal sesamoid bone (PSB). The μCT regions of interest (μROIs) are as follows: central subchondral (CS), central subchondral border (CSB), proximal subchondral μROI (PS), and trabecular μROI (TB). The CS μROI surrounded the lesion, if present, or was a 0.09 cm^2 semicircle at 39% of the proximodistal height (i.e., average lesion size and location in CLI-PSBs). The CSB μROI was a 1 mm-thick border around the CS μROI. The PS μROI was a 0.06 cm^2 semicircle whose distal edge was 0.5 mm from the proximal edge of the CS μROI. The TB μROI was a 0.60 cm^2 square drawn 5 mm from the subchondral bone surface and the proximal PSB border. (B) Basic fuchsin-stained section from a CLI-PSB showing histology ROIs (hROIs) in a CLI-PSB. The six hROIs are as follows: PS hROI (PS), CS hROI (CS), distal subchondral hROI (DS), proximal deep hROI (PD), central deep hROI (CD), and distal deep hROI (DD). Mean hROI area was 7.9 mm^2 in FX-PSB, 8.7 mm^2 in CLI-PSBs, and 8.8 mm^2 in CTRL-PSBs; in FX-PSBs, tissue gaps were excluded from hROI and μROI areas

Microdamage was not assessed for two CTRL-PSBs, as the tissue was inadvertently destroyed during grinding.

Subchondral bone microcracks (Cr) were defined as deeply stained linear features with a surrounding halo of basic fuchsin.[23] Calcified cartilage microcracks (Md.Cg.Cr) were defined as linear features extending from the tidemark with a surrounding halo of dark staining in subchondral hROIs.[19] The number of microcracks (N.Cr, N.Md.Cg.Cr), length of individual microcracks (Cr.Le, Md.Cg.Cr.Le), microcrack length sum (ΣCr.Le, ΣMd.Cg.Cr.Le where summation is zero in the absence of cracks), proximal angle between articular surface and calcified cartilage microcrack, hROI area (B.Ar), and articular surface length (Cg.Bd) were quantified. The microcrack areal density (N.Cr/B.Ar; number/mm^2), microcrack length per area (ΣCr.Le/B.Ar; mm/mm^2), average microcrack length (ΣCr.Le/N.Cr; mm), calcified cartilage crack number per articular surface length (N.Md.Cg.Cr/Cg.Bd; number/mm^2), average calcified cartilage crack length (ΣMd.Cg.Cr.Le/N.Md.Cg.Cr; mm), average proximal angle (degrees), and calcified cartilage crack length per articular surface length (ΣMd.Cg.Cr.Le/Cg.Bd; mm/mm) were derived. Whole bone microcrack variables were estimated by combining data from all hROIs.

Measurement repeatability for N.Md.Cg.Cr and N.Cr was tested by interrater reliability (IRR; Shrout-Fleiss fixed set reliability statistic), *t* tests, and Bland–Altman plots. N.Cr IRR was 0.65–0.92 among hROIs and 0.92 for whole bone; N.Md.Cg.Cr IRR was 0.79–0.96 among hROIs and 0.95 for whole bone. No significant differences ($p \le 0.05$) or biases were observed.

2.5 | Statistical analysis

Exercise history variables were compared between Groups (Case, Control) using a two-sided *t*-test or Wilcoxon test depending on data normality (Shapiro–Wilks statistic, $W \ge 0.9$). The effects of Group (CLI, CTRL, and FX-PSB) and µROI or hROI on densitometric and microcrack variables were assessed using analysis of variance (ANOVA) or ranked ANOVA depending on ANOVA residual normality (SAS 9.4; proc mixed).[1] Group, ROI, and their interaction were fixed effects and horse was a random effect. The effects of a lesion (present and absent) and ROI on densitometric and microcrack variables were similarly assessed. Linear regression was used to assess the relationships between microdamage and densitometric measures in the following (µROI and hROI) pairs: (CS and CS), (PS and PS), (whole bone and CS), and (whole bone and TB). The relationships between densitometric and microcrack variables with exercise history variables were determined using robust linear regressions (SAS 9.4) using data from CLI and CTRL-PSBs in all µROIs and the CS, PS, PD, and whole bone hROIs.[24] The relationships between the presence of calcified cartilage cracks and exercise history were assessed using univariate logistic regressions, as 60% of samples had N.Md.Cg.Cr = 0. For all analyses, $p \le 0.05$ was considered statistically significant.

3 | RESULTS

Averaged over µROIs, mean TMD was lower in FX-PSBs than CLI-PSBs. Averaged over Groups, AMD, TMD, and BVF differed among µROIs (Table S-B1). The interaction between Group and µROI was significant for AMD and BVF (Table 1).

Group densitometric differences were observed in the CS and TB µROIs (Table 1 and S-B1). BVF, TMD, and AMD in the CS µROI were 9%, 8%, and 3% lower in the FX-PSB compared with CTRL-PSBs. However, BVF, AMD, and TMD in the CS µROI of CLI-PSBs had intermediate values similar to CTRL-PSBs. In contrast, AMD in the TB µROI was 6% lower in CTRL-PSBs than in CLI-PSBs.

Regional densitometric differences within Groups were most apparent in FX-PSBs and CLI-PSBs (Table 1). BVF, AMD, and TMD were lowest in the CS µROI of FX-PSBs and CLI-PSBs. In FX-PSBs, the CS µROI BVF was 10.1% lower than in the CSB µROI and 6.8% lower than in the PS µROI. In contrast, CTRL-PSBs TB µROI BVF was nearly 8% lower than all other CTRL µROIs and no differences were apparent for AMD among all CTRL µROIs.

All PSBs contained subchondral bone microcracks. The fracture line passed through the CD hROI in all FX-PSBs, the CS in 9/10 FX-PSBs, the PD in 2/10 FX-PSBs, and the PS in 1/10 FX-PSBs. Regardless of Group, microdamage was greatest in the CS, PS, and CD hROIs and least in PD and DD hROIs (Table 2, Figure 3, and Table S-B2 and S-B3). The CS and PS hROI N.Cr and N.Cr/B.Ar were not significantly different among Groups; however, the ΣCr.Le/N.Cr in FX-PSB CS hROI was 41% higher compared with CTRL or CLI-PSBs, and FX-PSB CD hROI N.Cr/B.Ar was 65% higher than in CTRL-PSBs.

Calcified cartilage microcracks were more numerous and larger in Case PSBs (CLI and FX-PSB) than in CTRL-PSBs (Tables S-B2 and S-B3); they were found in 10/10 FX-PSBs, 9/10 CLI-PSBs, and 2/10 CTRL-PSBs. Case PSBs CS hROI had higher N.Md.Cg.Cr, N.Md.Cg.Cr/Cg.Bd, ΣMd.Cg.Cr.Le/N.Md.Cg.Cr, and ΣMd.Cg.Cr.Le/Cg.Bd than the CTRL-PSBs (Table 3). In the PS and DS hROIs, calcified cartilage variables were not different among Groups (Table 3). Although not statistically different, the mean proximal angle changed from being >100° in the PS and CS hROIs to ~56° in the DS hROI (Table S-B2).

3.1 | Densitometric and microdamage results by the presence of subchondral bone lesion

Densitometric and microdamage observations in PSBs with or without a lesion largely paralleled Group differences. Most Case horses (9/10 horses) had a subchondral lesion in the FX-PSB. The subchondral lesions were bilateral (found in FX and CLI-PSB) in 7/10 Case horses and unilateral (FX-PSB only) in 2/10 Case horses.[4] Lesions were not observed in CTRL-PSBs.[4]

The greatest differences between PSBs with, and without, a lesion occurred in the CS and TB ROIs (Tables S-B4 and SB-5). The CS µROI of PSBs with a lesion had 7.5% lower BVF, 7.8% lower AMD, and 2.8% lower TMD than PSBs without a lesion. The TB BVF in PSBs

TABLE 1 Least-square means ± SE from ANOVA or raw means ± SD from ranked ANOVA[¶] for tissue properties in each ROI in all three study groups

ROI	BVF[¶,†,‡] CTRL*	CLI*	FX*
Central subchondral*	0.98 (0.04)$_{\alpha}^{A}$	0.96 (0.04)$_{\alpha,\beta}^{A}$	0.90 (0.09)$_{\beta}^{A}$
Central subchondral border	0.97 (0.05)$_{\alpha}^{A}$	0.98 (0.05)$_{\alpha}^{B}$	0.99 (0.01)$_{\alpha}^{B}$
Trabecular	0.90 (0.09)$_{\alpha}^{B}$	0.97 (0.03)$_{\alpha}^{A}$	0.96 (0.03)$_{\alpha}^{A,B}$
Proximal subchondral	0.97 (0.04)$_{\alpha}^{A}$	0.96 (0.07)$_{\alpha}^{A,B}$	0.96 (0.07)$_{\alpha}^{B}$
	AMD[†,‡] (mg HA/cc)		
	CTRL	CLI*	FX*
Central subchondral*	796.06 (13.40)$_{\alpha}^{A}$	782.19 (13.40)$_{\alpha}^{A}$	733.08 (13.40)$_{\beta}^{A}$
Central subchondral border	814.90 (13.40)$_{\alpha}^{A}$	822.67 (13.40)$_{\alpha}^{A,B}$	817.05 (13.40)$_{\alpha}^{B}$
Trabecular	782.41 (13.40)$_{\alpha}^{A}$	827.57 (13.40)$_{\beta}^{B}$	816.65 (13.40)$_{\alpha,\beta}^{B}$
Proximal subchondral	791.75 (13.40)$_{\alpha}^{A}$	795.41 (13.40)$_{\alpha}^{A,B}$	786.66 (14.70)$_{\alpha}^{B}$
	TMD[†,§] (mg HA/cc)		
	CTRL*	CLI*	FX*
Central subchondral*	812.37 (5.79)$_{\alpha}^{A}$	809.15 (5.79)$_{\alpha}^{A}$	790.55 (5.79)$_{\beta}^{A}$
Central subchondral border	837.61 (5.79)$_{\alpha}^{B}$	838.84 (5.79)$_{\alpha}^{B}$	830.26 (5.79)$_{\alpha}^{B,C}$
Trabecular	843.47 (5.79)$_{\alpha}^{B}$	852.94 (5.79)$_{\alpha}^{B}$	842.63 (5.79)$_{\alpha}^{B}$
Proximal subchondral	811.62 (5.79)$_{\alpha}^{A}$	819.54 (5.79)$_{\alpha}^{A}$	812.77 (6.32)$_{\alpha}^{C}$

Note: Significant ANOVA effects are indicated by variable superscripts: †(ROI), §(Group), and ‡(Group × ROI). Pairwise comparisons of ROIs within a group (down column) are indicated by superscripts (A, B, and C). Pairwise comparisons of Groups for each ROI (across row) are indicated by subscripts (α and β). For all comparisons, significant comparisons are indicated by * and variables that do not share a superscript are significantly different at $p < 0.05$.

Abbreviations: AMD, apparent mineral density; ANOVA, analysis of variance; BVF, bone volume fraction; CLI, case contralateral intact group; CTRL, control group; FX, case fractured group; ROI, region of interest; TMD, tissue mineral density.

with a lesion were significantly higher than those without. In PSBs with a lesion, N.Cr and N.Cr/B.Ar were highest in the CS hROI; however, N.Cr and N.Cr/B.Ar were not different in the three subchondral hROIs of PSBs without a lesion. Calcified cartilage cracks were found in 16/16 PSBs with a lesion and 5/14 PSBs without a lesion. Additionally, BVF in the PS and CSB μROIs were higher in PSBs with a lesion than those without.

3.2 | Relationship between microcracks and densitometric measures

Variance in whole bone N.Md.Cg.Cr/Cg.Bd explained the largest amount of variance for BVF, AMD, and TMD in the CS μROI (Table 4). Whole bone and CS hROI N.Md.Cg.Cr and N.Md.Cg.Cr/Cg.Bd were negatively related to CS μROI TMD, AMD, and BVF.

3.3 | Differences in exercise history among Case and Control racehorses

Case horses participated in over twice as many lifetime works and events, accumulated nearly twice the lifetime work and event distance, had over twice as much time in training since last layup, and performed nearly twice the distance, events, and works each month, 1–12 months before death (Table 5). Average event distances and race variables were not different between Case and Control horses. Other exercise intensity variables were not different or had marginally insignificant differences between Case and Controls groups ($0.10 \le p < 0.05$; Table S-A2).

3.4 | Relationships between exercise history, microcracks, and densitometry

The directions of the regressions between BVF and AMD with exercise intensity, layup, and exercise intensity in the year before death in the CS ROIs differed from other regions and was most apparent between the CS and TB μROIs (Figure 4). In the CS μROI, BVF and AMD decreased with exercise intensity (e.g., increasing with days between activities; $0.07 \le R^2 \le 0.12$), BVF decreased with events and works 2–12 months before death ($0.09 \le R^2 \le 0.12$), and AMD increased with time in layup ($R^2 = 0.10$). Conversely, in the TB μROI, BVF increased with exercise intensity ($R^2 = 0.17$), BVF decreased with time in layup ($0.10 \le R^2 \le 0.15$), and BVF and AMD decreased with time elapsed

TABLE 2 Raw means (SD) of microdamage variables for group and ROI

	N.Cr† (#)		
	CTRL*	CLI*	FX*
Proximal subchondral	11.0 (11.3)$_{\alpha}^{A,B}$	29.1 (33.7)$_{\alpha}^{A,B}$	13.7 (15.0)$_{\alpha}^{B,C}$
Central subchondral	19.8 (22.0)$_{\alpha}^{A}$	52.0 (39.0)$_{\alpha}^{A}$	60.9 (40.5)$_{\alpha}^{A}$
Distal subchondral	6.1 (9.7)$_{\alpha}^{B,C}$	11.6 (13.4)$_{\alpha}^{B,C}$	9.4 (7.3)$_{\alpha}^{B,C}$
Proximal deep	4.3 (4.9)$_{\alpha}^{C,D}$	4.9 (5.8)$_{\alpha}^{B,C}$	3.0 (3.0)$_{\alpha}^{D,C}$
Central deep	6.9 (9.7)$_{\beta}^{A,B}$	14.5 (10.8)$_{\alpha,\beta}^{A,B,C}$	15.6 (9.4)$_{\alpha}^{A,B}$
Distal deep	2.2 (3.2)$_{\alpha}^{D}$	1.5 (3.3)$_{\alpha}^{C}$	2.0 (2.4)$_{\alpha}^{D}$
	N.Cr/B.Ar† (#/mm^2)		
	CTRL*	CLI*	FX*
Proximal subchondral	1.1 (1.0) $_{\alpha}^{A,B}$	3.1 (3.4)$_{\alpha}^{A,B}$	1.6 (1.5)$_{\alpha}^{B,C}$
Central subchondral	2.1 (2.1)$_{\alpha}^{A}$	6.0 (4.1)$_{\alpha}^{A}$	7.6 (5.1)$_{\alpha}^{A}$
Distal subchondral	0.6 (1.0)$_{\alpha}^{B,C}$	1.3 (1.4)$_{\alpha}^{B,C}$	1.3 (1.1)$_{\alpha}^{B,C}$
Proximal deep	0.4 (0.5)$_{\alpha}^{B,C}$	0.5 (0.6)$_{\alpha}^{C,D}$	0.4 (0.5)$_{\alpha}^{D,C}$
Central deep*	0.7 (0.9)$_{\beta}^{A,B,C}$	1.6 (1.0)$_{\alpha,\beta}^{A,B}$	2.0 (1.2)$_{\alpha}^{A,B}$
Distal deep	0.2 (0.3)$_{\alpha}^{C}$	0.2 (0.4)$_{\alpha}^{D}$	0.3 (0.4)$_{\alpha}^{D}$
	ΣCr.Le/N.Cr†,§ (mm)		
	CTRL	CLI*	FX*
Proximal subchondral	0.07 (0.02)$_{\alpha}^{A}$	0.07 (0.04)$_{\alpha}^{A}$	0.06 (0.03)$_{\alpha}^{B,C}$
Central subchondral*	0.07 (0.02)$_{\alpha}^{A}$	0.07 (0.03)$_{\alpha}^{A}$	0.12 (0.05)$_{\beta}^{A}$
Distal subchondral	0.04 (0.04)$_{\alpha}^{A}$	0.05 (0.03)$_{\alpha}^{A,B}$	0.04 (0.03)$_{\alpha}^{C}$
Proximal deep	0.05 (0.04)$_{\alpha}^{A}$	0.03 (0.03)$_{\alpha}^{A,B}$	0.07 (0.06)$_{\alpha}^{A,B,C}$
Central deep	0.07 (0.05)$_{\alpha}^{A}$	0.07 (0.04)$_{\alpha}^{A,B}$	0.10 (0.06)$_{\alpha}^{A,B}$
Distal deep	0.05 (0.07)$_{\alpha}^{A}$	0.02 (0.03)$_{\alpha}^{B}$	0.05 (0.06)$_{\alpha}^{C}$
	ΣCr.Le/B.Ar† (mm/mm^2)		
	CTRL*	CLI*	FX*
Proximal subchondral	0.09 (0.10)$_{\alpha}^{A,B}$	0.27 (0.34)$_{\alpha}^{A,B}$	0.12 (0.14)$_{\alpha}^{B,C}$
Central subchondral*	0.17 (0.22)$_{\beta}^{A}$	0.50 (0.36)$_{\alpha,\beta}^{A}$	0.91 (0.54)$_{\alpha}^{A}$
Distal subchondral	0.06 (0.11)$_{\alpha}^{B}$	0.08 (0.08)$_{\alpha}^{B,C}$	0.08 (0.08)$_{\alpha}^{B,C,D}$
Proximal deep	0.03 (0.03)$_{\alpha}^{B}$	0.03 (0.03)$_{\alpha}^{D,C}$	0.05 (0.08)$_{\alpha}^{C,D}$
Central deep*	0.06 (0.09)$_{\beta}^{A,B}$	0.11 (0.07)$_{\alpha,\beta}^{A,B}$	0.19 (0.14)$_{\alpha}^{A,B}$
Distal deep	0.02 (0.03)$_{\alpha}^{B}$	0.01 (0.02)$_{\alpha}^{D}$	0.02 (0.03)$_{\alpha}^{D}$

Note: Significant ANOVA effects indicated by variable superscripts: †(ROI), §(Group), and ‡(Group × ROI). Pairwise comparisons of ROIs within a group (down column) are indicated by letters (A, B, C, and D). Pairwise comparisons of Groups within each ROI (across row) are indicated by greek letters (α and β). For all comparisons, significance is indicated by * and variables that do not share a superscript are significantly different at $p \le 0.05$.

Abbreviations: ANOVA, analysis of variance; CLI, case contralateral intact group; CTRL, control group; FX, case fractured group; N.Cr, microcrack number; N.Cr/B.Ar, microcrack density; ΣCr.Le/B.Ar, microcrack length per area; ΣCr.Le/N.Cr, average microcrack length; ROI, region of interest.

between death and the previous event ($R^2 = 0.34, 0.39$). When significant, BVF decreased with lifetime measures in both the CS and TB μROIs (Table S-A3). CS μROI AMD had no significant relationships to lifetime summary measures; AMD increased with horse age in the PS and CSB μROIs ($R^2 = 0.18, 0.13$), and with age at start of training in the TB μROI ($R^2 = 0.20$).

In the CS and TB μROIs, TMD decreased with exercise intensity ($0.14 \le R^2 \le 0.27$). TMD increased with lifetime summary variables in the CS, CSB, and PS μROIs (Table S-A4). TMD was not associated with exercise in the year before death.

The relationships between microdamage and exercise in the CS hROI were different from those in the PS and PD hROIs, which had

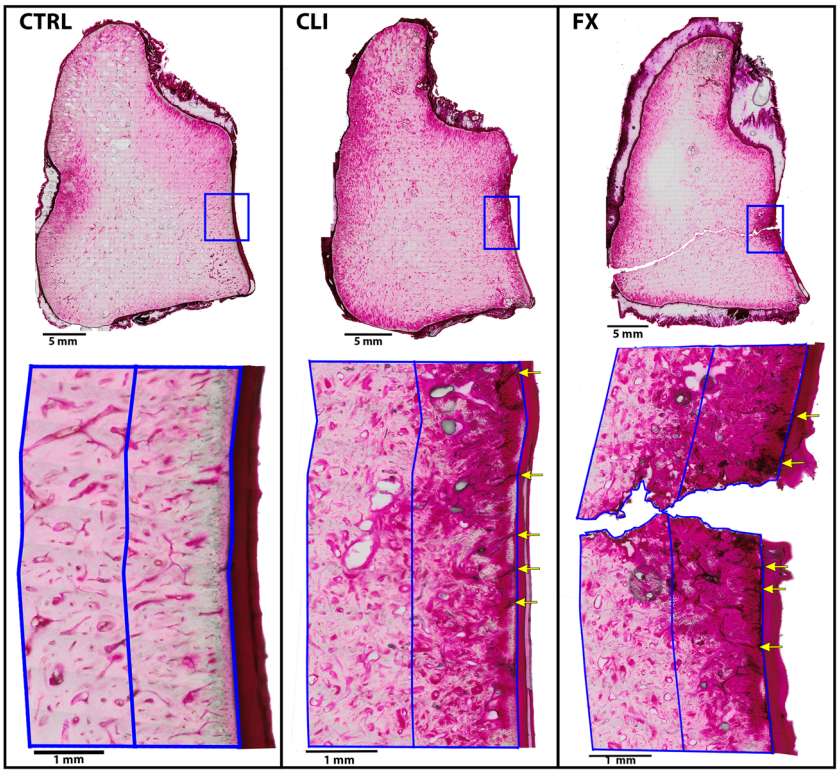

FIGURE 3 Basic fuchsin-stained histology sections showing internal and calcified cartilage microcracks on Control (CTRL; left), case contralateral intact (CLI; center), and case fractured (FX; right) proximal sesamoid bones (PSBs). The top row shows the entire stained sagittal section, where the box encompasses the central subchondral and central deep histology regions of interest (hROIs). The bottom row shows the central deep hROI and central subchondral hROI from the CTRL, CLI, and FX PSB in more detail. The arrows indicate calcified cartilage microcracks

low, but detectable, amounts of microdamage. In the CS hROI, N.Cr, N.Cr/B.Ar and ΣCr.Le/B.Ar increased with exercise frequency 2–4 months before death ($0.19 \le R^2 \le 0.29$); opposite of the relationships observed between BVF, AMD, and exercise intensity in the overlapping CS μROI. In the CS hROI, ΣCr.Le/B.Ar increased with time spent in layup ($R^2 = 0.18$). Events 1–2 months before death were the only predictors of presence of calcified cartilage cracks (Table S-A5).

Damage was not observed within the TB region; however, in the low damage PS and PD hROIs, N.Cr and N.Cr/B.Ar decreased with exercise intensity ($0.15 \le R^2 \le 0.36$) and in the PD hROI ΣCr.Le/B.Ar or ΣCr.Le/N.Cr decreased with exercise intensity 1–10 months before death ($0.15 \le R^2 \le 0.32$). In the PS and PD hROIs, N.Cr, N.Cr/B.Ar increased with time in layup ($0.14 \le R^2 \le 0.28$). A summary of all regressions is in Tables S-A3–S-A5.

4 | DISCUSSION

Medial PSBs from Thoroughbred racehorses that did (Case) and did not (Control) have a unilateral biaxial PSB fracture were evaluated for differences in tissue densitometric and microdamage measures at multiple locations, including the site of a radiolucent subchondral bone lesion.[4] In Case PSBs, the lesion site had higher N.Cr/B.Ar and lower BVF, AMD, and TMD compared with surrounding tissue. The lesion observed in Case PSBs is believed to precede PSB fracture and tended to be bilaterally present, these findings are consistent with previous reports.[4,25]

We hypothesize that the calcified cartilage cracks developed after the osteopenic lesion. Likely, the lesion reduced tissue stiffness, allowing greater deformation of and cracking in the calcified cartilage. Three observations support this hypothesis. First, calcified cartilage cracks were primarily observed in PSBs with a lesion. Second, reduced BVF was associated with more calcified cartilage cracks at the lesion site. Third, the probability of calcified cartilage cracks increased with exercise 1–2 months before death, while subchondral microcrack number and areal density increased with exercise 2–4 months before death. Similar observations have been associated with articular surface collapse of horses with palmar osteochondral disease.[26]

4.1 | Relationship of exercise to densitometric and microdamage variables

The relationships between BVF, N.Cr, N.Cr/B.Ar and exercise intensity variables were different for the CS and other ROIs. However, the relationships between tissue mineralization (TMD) and exercise intensity variables were similar among regions, providing an opportunity to infer how the rate terms in the conceptual model of bone remodeling (Figure 1) were related to exercise. Previous research indicates that osteoid formation rate (k_2), damage formation rate (k_4), undamaged mineralized bone resorption rate (k_1), and damaged bone resorption rate (k_5) likely depend on mechanical loading (e.g., strain magnitude and frequency) and, potentially, microdamage-induced inflammation.[10,27–30] Primary mineralization rate (k_3) may be independent of mechanical loading.[31,32] The exact dependencies of the rate constants on mechanical parameters are unknown. However, inferences about how rate terms were affected

TABLE 3 Raw means (SD) of calcified cartilage microcrack variables for Group and ROI

	N.Md.Cg.Cr†,§ (#)		
	CTRL	CLI*	FX*
Proximal subchondral	0.8 (1.5)$_{\alpha}^{A}$	2.0 (2.7)$_{\alpha}^{A,B}$	1.5 (1.5)$_{\alpha}^{A,B}$
Central subchondral*	0.1 (0.4)$_{\alpha}^{A}$	2.6 (2.4)$_{\beta}^{A}$	5.1 (4.1)$_{\beta}^{A}$
Distal subchondral	0.0 (0.0)$_{\alpha}^{A}$	0.3 (0.7)$_{\alpha}^{B}$	1.7 (2.6)$_{\alpha}^{B}$
	N.Md.Cg.Cr/Cg.Bd†,§ (#/mm)		
	CTRL	CLI*	FX*
Proximal subchondral	0.1 (0.2)$_{\alpha}^{A}$	0.3 (0.4)$_{\alpha}^{A,B}$	0.3 (0.2)$_{\alpha}^{A,B}$
Central subchondral*	0.0 (0.1)$_{\alpha}^{A}$	0.5 (0.5)$_{\beta}^{A}$	0.9 (0.6)$_{\beta}^{A}$
Distal subchondral	0.0 (0.0)$_{\alpha}^{A}$	0.1 (0.1)$_{\alpha}^{B}$	0.3 (0.5)$_{\alpha}^{B}$
	ΣMd.Cg.Cr.Le/N.Md.Cg.Cr†,§ (mm)		
	CTRL	CLI*	FX
Proximal subchondral	0.07 (0.15)$_{\alpha}^{A}$	0.12 (0.13)$_{\alpha}^{A,B}$	0.08 (0.08)$_{\alpha}^{A}$
Central subchondral*	0.01 (0.04)$_{\alpha}^{A}$	0.18 (0.16)$_{\beta}^{A}$	0.18 (0.11)$_{\beta}^{A}$
Distal subchondral	0.00 (0.00)$_{\alpha}^{A}$	0.06 (0.13)$_{\alpha}^{B}$	0.09 (0.15)$_{\alpha}^{A}$
	ΣMd.Cg.Cr.Le/Cg.Bd†,§ (mm/mm)		
	CTRL	CLI*	FX*
Proximal subchondral	0.03 (0.08)$_{\alpha}^{A}$	0.08 (0.11)$_{\alpha}^{A,B}$	0.03 (0.03)$_{\alpha}^{B}$
Central subchondral*	0.00 (0.01)$_{\alpha}^{A}$	0.12 (0.13)$_{\beta}^{A}$	0.17 (0.13)$_{\beta}^{A}$
Distal subchondral	0.00 (0.00)$_{\alpha}^{A}$	0.01 (0.03)$_{\alpha}^{B}$	0.09 (0.16)$_{\alpha}^{B}$

Note: Significant ANOVA effects indicated by variable superscripts: †(ROI), §(Group), and ‡(Group*ROI). Pairwise comparisons of ROIs within a group (down column) are indicated by letters (A and B). Pairwise comparisons of Groups for each ROI (across row), are indicated by subscripts (α and β). For all comparisons, significance is indicated by * and variables that do not share a superscript are significantly different at $p \le 0.05$.

Abbreviations: N.Md.Cg.Cr, calcified cartilage crack number; N.Md.Cg.Cr/Cg.Bd, number of calcified cartilage cracks per articular surface length; ΣMd.Cg.Cr.Le/Cg.Bd, calcified cartilage crack length per articular surface length; ΣMd.Cg.Cr.Le/N.Md.Cg.Cr, average calcified cartilage crack length; ROI, region of interest.

by mechanical loadings (i.e., exercise) can be made from the regression findings.

Two location-specific contradictory relationships were observed between exercise intensity variables and BVF. In the CS region, BVF decreased with exercise intensity and in the TB region BVF increased with lifetime exercise intensity (Figure 4). In the model, BVF is mineralized bone tissue per TV (BVF = BV_M/TV = (BV_D + BV_{UD})/TV). Additionally, N.Cr/B.Ar (related to BV_D/TV) was positively correlated to exercise intensity before death in the CS region, but in the TB region no microdamage was observed. Also, in the examined low damage regions N.Cr/B.Ar was negatively correlated to exercise intensity (Figure 4). These contradictory relationships are explained if the rate constants depend on exercise intensity in a location-specific manner. Location dependence could result from differences in strain magnitude or rate among the sites.

We hypothesize that the contradictory relationships observed are caused by the CS site unsuccessfully responding to microdamage induced by exercise in Case horses. Damage and damage-induced bone resorption resulted in increases in damaged bone (BV_D) and marrow space (MV) and decrease of BV_{UD}. Other locations successfully responded to exercise by increasing/maintaining BV_{UD} and maintaining a "low-enough" BV_D to prevent a damage feedback loop. In Control PSBs, which had no lesions, all locations successfully adapted to exercise levels. The model predicts solutions consistent with this hypothesis if rate constants are allowed to vary among sites. Damage formation rate (k_4) can be used to arrive at a consistent solution. The partial derivative of BV_D/TV with respect to damage formation rate (k_4) is positive and the partial derivative of BV_M/TV with respect to k_4 is negative if the damaged bone resorption rate (k_5) is higher than the turnover rate (k_1), a condition expected during normal targeted bone remodeling (Supporting Information C).[8,11] At steady-state, the model predicts a site with a higher damage formation rate (k_4) would have a higher BV_D/TV and lower BV_M/TV than a site with a lower k_4. That is, the model correctly predicts

TABLE 4 Linear regression slope (R^2) between microdamage and densitometric measures in the CS μROI with the CD hROI and whole bone hROIs

		CS hROI			
		N.Md.Cg.Cr (#)	N.Md.Cg.Cr/Cg.Bd (#/mm)	N.Cr (#)	N.Cr/B.Ar (#/mm^2)
CS μROI	AMD (mg HA/cc)	−7.55 (0.29)	−46.33 (0.31)	NS	NS
	TMD (mg HA/cc)	−2.86 (0.31)	−17.39 (0.33)	−0.19 (0.17)	−1.76 (0.21)
	BVF	−0.01 (0.23)	−0.06 (0.25)	NS	NS
		Whole bone microdamage			
CS μROI	AMD (mg HA/cc)	−6.2 (0.40)	−113.79 (0.45)	NS	NS
	TMD (mg HA/cc)	−2.06 (0.34)	−37.51 (0.37)	NS	NS
	BVF	−0.01 (0.36)	−0.15 (0.40)	NS	NS

Note: Reported regressions are significant at $p \le 0.05$; nonsignificant regressions are indicated by NS.

Abbreviations: AMD, apparent mineral density; BVF, bone volume fraction; CD, central deep; CS, central subchondral; hROI, histology region of interest; μROI, microcomputed tomography region of interest; N.Md.Cg.Cr, calcified cartilage crack number; N.Md.Cg.Cr/Cg.Bd, number of calcified cartilage cracks per articular surface length; N.Cr, microcrack number; N.Cr/B.Ar, microcrack density; NS, nonsignificant; TMD, tissue mineral density.

TABLE 5 Median (minimum, maximum) and mean (SD) of Case ($n = 10$) and Control ($n = 10$) exercise history variables

Variable type	Variable (unit)	Median (minimum, maximum)		Mean (SD)	
		Case	Control	Case	Control
Lifetime exercise	Age[a] (years)	3.54 (2.34, 7.84)	3.38 (2.61, 7.37)	3.95[A] (1.58)	3.81[A] (1.53)
	Number of events[a] (events)	28.0 (14.00, 153.00)	15.50 (4.00, 78.00)	43.60[A] (41.19)	24.60[B] (23.68)
	Number of races[a] (races)	8.00 (0.00, 32.00)	5.00 (0.00, 26.00)	10.70[A] (9.92)	7.00[A] (8.38)
	Number of works[a] (works)	19.50 (12.00, 121.00)	10.50 (4.00, 52.00)	32.90[A] (32.76)	17.60[B] (15.83)
Exercise intensity	Days between events (days)	11.95 (7.83, 20.61)	17.54 (8.08, 41.85)	12.52[A] (4.09)	19.90[Ab] (10.20)
	Days between events during active training[a] (days)	8.96 (7.83, 16.5)	11.34 (7.85, 13.78)	10.01[A] (2.67)	10.87[A] (2.34)
	Furlongs per month (furlong/mo)	8.96 (2.99, 16.18)	4.57 (2.76, 10.69)	8.81[A] (3.57)	5.89[A] (2.78)
	Furlongs per month of active training (furlong/mo)	11.15 (2.99, 16.18)	9.05 (4.54, 15.51)	10.68[A] (3.49)	9.76[A] (4.11)
Layup	Layup time[a] (days)	87.5 (0.00, 698.00)	62.00 (0.00, 927.00)	136.6[A] (211.02)	234[A] (330.02)
	Average layup length[a] (days)	87.50 (0.00, 201.00)	55.25 (0, 323)	84.25[A] (81.39)	106.75[A] (130.74)
	Percent career in layup[a] (%)	19.43 (0.00, 42.41)	24.36 (0.00, 81.25)	16.99[A] (16.05)	30.92[A] (33.86)
	Time since end of last layup (days)	256.00 (61, 461)	94.00 (0.00, 237.00)	259.90[A] (139.86)	104.70[B] (81.04)
	Events since last layup (events)	28.00 (8.00, 49.00)	10.00 (0.00, 26.00)	27.60[A] (13.48)	10.40[B] (8.64)
Exercise before death	Events 1 month before death (events)	3.00 (2.00, 5.00)	2.00 (0.00, 4.00)	3.30[A] (0.95)	1.90[B] (1.29)
	Events 2 months before death (events)	6.00 (3.00, 9.00)	4.00 (0.00, 7.00)	5.90[A] (1.91)	3.50[B] (2.32)
	Events 4 months before death (events)	12.50 (8.00, 17.00)	8.00 (0.00, 14.00)	12.00[A] (3.20)	7.20[B] (5.12)
	Events 6 months before death (events)	18.00 (11.00, 23.00)	10.00 (0.00, 22.00)	17.40[A] (4.06)	9.90[B] (6.67)
	Events 8 months before death[a] (events)	22.00 (14.00, 29.00)	10.50 (1.00, 26.00)	21.40[A] (6.33)	11.60[B] (7.68)
	Events 10 months before death[a] (events)	24.00 (14.00, 35.00)	11.00 (2.00, 26)	24.70[A] (8.21)	11.80[B] (7.51)
	Events 1 year before death[a] (events)	24.50 (14.00, 41.00)	11.00 (4.00, 26)	27.10[A] (10.40)	12.20[B] (7.02)

Note: Within a row, Group means that share a superscript (A and B) are not significantly different at $p \leq 0.05$. Variable definitions and full results are given in Supporting Information A.

[a]Nonnormal distributions.

[b]Marginal significance at $p < 0.10$.

observed morphological differences in the CS and TB sites if the mechanical damage rate is higher in the former compared to the latter site.

In the TB region bone damage was not detected, but the BVF in horses with a lesion was higher than those without a lesion. In the model, $BV_D/TV = 0$ is predicted if the damage formation rate (k_4) is zero and non-zero BV_{UD}/TV is predicted if the other rate constants are non-zero. Damage formation rate (k_4) increases with tissue stress and, therefore, would be different at the subchondral and TB tissue sites if respective stresses are different. In support of this hypothesis, previous research indicates that subchondral tissues experience a localized higher stress magnitude than deeper tissues,[33] that shear stresses resulting from the contact stress cause linear microcracks like those observed in the CS site,[34] and that Young's modulus increases with BVF[35] and decreases with N.Cr/B.Ar.[36] So, there is likely a stress difference between the two regions that is exacerbated when the BVF at the CS site is low. This low BVF CS site may act as a stress riser, causing a further increase in the damage formation rate (k_4). Regional dependencies on the other rate constants may exist, but a full analysis is beyond the scope of this study. To fully test this set of hypotheses, a stress analysis model coupled with the proposed turnover model is needed.

Unlike BVF, TMD decreased with event frequency regardless of location. TMD is the extent of mineralization of the mineralized bone volume ($BV_M = BV_{UD} + BV_D$). In this model, k_3 represents the rate of primary mineralization of bone, so BV_M is bone that had reached primary mineralization. Secondary mineralization is not explicitly included in the model but depends on elapsed time between initial mineralization and resorption of the mineralized tissue. In a steady-state model (as presented here) the rate at which tissue "cycles" through a compartment depends on the magnitudes of the rate constants, but not upon their ratios. The negative correlation of TMD with event frequency, therefore, suggests that at all sites the "cycle rate" is increased by event frequency. At a high cycle rate tissue

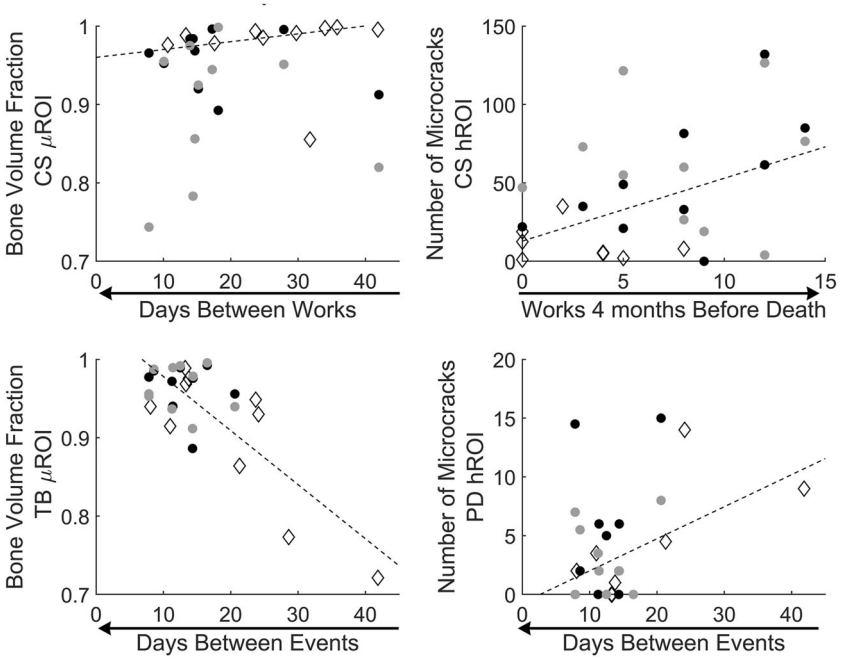

FIGURE 4 Selected exercise robust linear regressions for bone volume fraction (BVF) and number of subchondral microcracks (N.Cr). In all panels, the arrow below the *x* axis title shows the direction of increasing exercise intensity. Data from case contralateral limb intact (CLI) PSBs are shown with the black filled circle, case fractured (FX) PSBs with the gray filled circle, and control with the open diamond; only CLI-PSB and CTRL-PSB data were used to build the robust linear regressions. In the central subchondral region of interest, BVF decreased with an increase in exercise intensity (or with fewer days between works; $R^2 = 0.10$) and N.Cr increased with exercise intensity ($R^2 = 0.18$). In the trabecular microcomputed tomography region of interest, BVF decreased with a decrease in exercise intensity (or with more days between events; $R^2 = 0.17$). In the proximal deep histology region of interest, N.Cr decreased with exercise intensity ($R^2 = 0.17$)

remains in a mineralizing compartment (i.e., BV_D or BV_{UD}) for less time, so mineralization has less time to proceed, and TMD is reduced. The reduced TMD observed at the lesion site, compared with other regions, suggests a higher turnover rate at the lesion site. This hypothesis is consistent with the observation that TMD increases with tissue age and decreases with tissue turnover rate.[37,38]

Exercise intensity variables and layup variables were the best predictors of densitometric and microdamage measures. Rate of loading and the difference between applied and habitual loads affect bone formation, bone turnover, damage formation, and damage repair rates.[27–29,32] Exercise intensity variables reflect load application rate, whereas layup variables reflect changes in load magnitude from a habitual condition; so, the observed relationships between these variable types and measured densitometric and microdamage variables are consistent with previous research.[8]

Exercise intensity variables were expressed as either activities per time or distance per time. These somewhat correlated measures may have different effects on bone biology and thus the rate constants. The response of bone cells to mechanical loading saturates rapidly after loading begins.[29] Therefore, if saturation occurs early in an exercise event, event frequency variables may be better suited to drive osteoid formation rate (k_2) than distance frequency. However, fatigue damage is related to the total number of applied load cycles. When combined with average stride length, distance frequency

FIGURE 5 Magnetic resonance image of the left fetlock joint of living racehorse from a different racing population (outside United States) showing a bone bruise in the same location (arrow) as the density lesions identified in this study. Increased signal indicates active bone remodeling at the lesion site. This horse suffered low-level intermittent lameness, but no other clinical symptoms. This image is used with permission of Drs. Weir, Riggs, and Stewart

variables indicate number of load cycles, so distance frequency variables may be better suited to drive damage formation rate (k_4). Study results neither support nor refute this hypothesis, as both event and distance frequency variables were related to densitometric and microcrack data.

Limitations of this study include examination of only medial PSBs from a small sample of racehorses in one geographic population. Medial PSBs were selected because unilateral PSB fracture is more common in medial than lateral PSBs and subchondral lesions have previously been reported in medial PSBs.[4,25] Examination of PSBs from only California Thoroughbred racehorses limits the extent to which results can be generalized to other racehorses. However, similar changes have been reported or clinically observed (Figure 5) in other racing populations.[25]

An abaxial region of focal osteopenia and high microdamage was observed in racehorses that were euthanized after incurring unilateral biaxial PSB fracture; these focal changes were not observed in racehorses killed during training from other injuries. The densitometric properties and microdamage measures within this bone lesion site had different relationships to exercise compared with other sites within the bone. A compartmental model of bone's tissue turnover cycle was introduced and used to understand the site-specific differences in densitometric and microdamage measures, and in the relationships of those measures to exercise.

ACKNOWLEDGMENTS

This project was supported by the Grayson Jockey Club Research Foundation, Inc., the Maury Hull Fellowship (University of California Davis), the Louis R. Rowan Fellowship (California Thoroughbred Foundation), the University of California Davis Center for Equine Health (with funds provided by the State of California satellite wagering fund and contributions by private donors).

AUTHOR CONTRIBUTIONS

All authors have read and approved the final manuscript for submission. Sarah K. Shaffer and Tanya C. Garcia were responsible for data collection and collection methods. Sarah K. Shaffer also aided in research design, data analysis, interpretation, and manuscript drafting. Drs. Susan M. Stover and David P. Fyhrie assisted with research design, data interpretation, and manuscript drafting.

ORCID

Sarah K. Shaffer http://orcid.org/0000-0002-8361-7385
Tanya C. Garcia https://orcid.org/0000-0001-6137-6085
Susan M. Stover https://orcid.org/0000-0002-2111-7887
David P. Fyhrie https://orcid.org/0000-0002-2558-5960

REFERENCES

1. Ferry AT, Graves T, Theodore GH, Gill TJ. Stress fractures in athletes. *Phys Sportsmed*. 2010;38(2):109-116.
2. Martig S, Chen W, Lee PVS, Whitton RC. Bone fatigue and its implications for injuries in racehorses. *Equine Vet J*. 2014;46(4):408-415.
3. Stover SM. The epidemiology of thoroughbred racehorse injuries. *Clin Tech Equine Pract*. 2003;2(4):312-322.
4. Shaffer SK, To C, Garcia TC, Fyhrie DP, Uzal FA, Stover SM. Subchondral focal osteopenia associated with proximal sesamoid bone fracture in Thoroughbred racehorses. *Equine Vet J*. 2021;53(2):294-305. doi:10.1111/evj.13291
5. Anthenill LA, Stover SM, Gardner IA, et al. Association between findings on palmarodorsal radiographic images and detection of a fracture in the proximal sesamoid bones of forelimbs obtained from cadavers of racing Thoroughbreds. *Am J Vet Res*. 2006;67(5):858-868. doi:10.2460/ajvr.67.5.858
6. Riggs CM. Fractures—a preventable hazard of racing thoroughbreds? *Vet J*. 2002;163(1):19-29.
7. Anthenill LA, Stover SM, Gardner IA, Hill AE. Risk factors for proximal sesamoid bone fractures associated with exercise history and horseshoe characteristics in Thoroughbred racehorses. *Am J Vet Res*. 2007;68(7):760-771. doi:10.2460/ajvr.68.7.760
8. Robling AG, Fuchs RK, Burr DB. Mechanical adaptation. *Basic and applied bone biology*. Elsevier; 2014:175-204. https://linkinghub.elsevier.com/retrieve/pii/B9780124160156000095
9. Martin RB. The role of bone remodeling in preventing or promoting stress fractures. In: Burr DD, Milgrom C, eds. *Musculoskeletal fatigue and stress fractures*. CRC Press, Inc; 2001:183-203.
10. Martin RB, Burr DB, Sharkey NA, Fyhrie DP. *Mechanical adaptability of the skeleton*. Vol 275, 2nd ed. Springer; 2015:343. http://link.springer.com/10.1007/978-1-4939-3002-9
11. Robling AG, Castillo AB, Turner CH. Biomechanical and molecular regulation of bone remodeling. *Annu Rev Biomed Eng*. 2006;8(1):455-498. http://www.annualreviews.org/doi/10.1146/annurev.bioeng.8.061505.095721
12. Murshed M. Mechanism of bone mineralization. *Cold Spring Harb Perspect Med*. 2018;8(12):1-11.
13. Hernandez CJ, Gupta A, Keaveny TM. A biomechanical analysis of the effects of resorption cavities on cancellous bone strength. *J Bone Miner Res*. 2006;21(8):1248-1255. doi:10.1359/jbmr.060514
14. Hughes JM, Popp KL, Yanovich R, Bouxsein ML, Matheny RW Jr. The role of adaptive bone formation in the etiology of stress fracture. *Exp Biol Med*. 2017;242(9):897-906.
15. van Oers RFM, van Rietbergen B, Ito K, Huiskes R, Hilbers PAJ. Simulations of trabecular remodeling and fatigue: Is remodeling helpful or harmful? *Bone*. 2011;48(5):1210-1215. doi:10.1016/j.bone.2011.01.011.
16. Hodsman AB, Kisiel M, Adachi JD, Fraher LJ, Watson PH. Histomorphometric evidence for increased bone turnover without change in cortical thickness or porosity after 2 years of cyclical hPTH(1-34) therapy in women with severe osteoporosis. *Bone*. 2000;27(2):311-318. https://linkinghub.elsevier.com/retrieve/pii/S8756328200003161
17. Bradbeer JN, Arlot ME, Meunler PJ, Reeve J. Treatment of osteoporosis with parathyroid peptide (hPTH 1–34) and oestrogen: increase in volumetric density of iliac cancellous bone may depend on reduced trabecular spacing as well as increased thickness of packets of newly formed bone. *Clin Endocrinol*. 1992;37(3):282-289.
18. Dempster DW, Compston JE, Drezner MK, et al. Standardized nomenclature, symbols, and units for bone histomorphometry: a 2012 update of the report of the ASBMR Histomorphometry Nomenclature Committee. *J Bone Miner Res*. 2013;28(1):2-17.
19. Whitton RC, Ayodele BA, Hitchens PL, Mackie EJ. Subchondral bone microdamage accumulation in distal metacarpus of Thoroughbred racehorses. *Equine Vet J*. 2018;50(6):766-773.
20. Kristoffersen M, Hetzel U, Parkin TDH, Singer ER. Are bi-axial proximal sesamoid bone fractures in the british thoroughbred racehorse a bone fatigue related fracture? A histological study. *Vet Comp Orthop Traumatol*. 2010;23(5):336-342.

21. Burr DB, Hooser M. Alterations to the en bloc basic fuchsin staining protocol for the demonstration of microdamage produced in vivo. *Bone*. 1995;17(4):431-433.
22. Schneider CA, Rasband WS, Eliceiri KW. NIH Image to ImageJ: 25 years of image analysis. *Nat Methods*. 2012;9(7):671-675.
23. Lee TC, Mohsin S, Taylor D, et al. Detecting microdamage in bone. *J Anat*. 2003;203(2):161-172.
24. Greco L, Luta G, Krzywinski M, Altman N. Analyzing outliers: robust methods to the rescue. *Nat Methods*. 2019;16(4):275-276.
25. Ayodele BA, Hitchens PL, Wong ASM, Mackie EJ, Whitton RC. Microstructural properties of the proximal sesamoid bones of Thoroughbred racehorses in training. *Equine Vet J*. 2020;53:1-9.
26. Bani Hassan E, Mirams M, Ghasem-Zadeh A, et al. Role of subchondral bone remodelling in collapse of the articular surface of Thoroughbred racehorses with palmar osteochondral disease. *Equine Vet J*. 2016;48:228-233. https://onlinelibrary.wiley.com/doi/10.1111/evj.12415
27. Rubin C, Lanyon L. Bone remodeling in response to applied dynamic loads. *J Bone Jt Surg*. 1984;66-A3:397-402.
28. Lanyon LE. Functional strain as a determinant for bone remodeling. *Calcif Tissue Int*. 1984;36(1 Suppl):56-61.
29. Turner CH. Three rules for bone adaptation to mechanical stimuli. *Bone*. 1998;23(5):399-407.
30. Loi F, Córdova LA, Pajarinen J, Lin TH, Yao Z, Goodman SB. Inflammation, fracture and bone repair. *Bone*. 2016;86:119-130.
31. Suniaga S, Rolvien T, vom Scheidt A, et al. Increased mechanical loading through controlled swimming exercise induces bone formation and mineralization in adult zebrafish. *Sci Rep*. 2018;8(1):3646. http://www.nature.com/articles/s41598-018-21776-1
32. Robling AG, Burr DB, Turner CH. Recovery periods restore mechanosensitivity to dynamically loaded bone. *J Exp Biol*. 2001;204(19):3389-3399.
33. Eberhardt AW, Keer LM, Lewis JL, Vithoontien V. An analytical model of joint contact. *J Biomech Eng*. 1990;112(4):407-413.
34. Boyce TM, Fyhrie DP, Glotkowski MC, Radin EL, Schaffler MB. Damage type and strain mode associations in human compact bone bending fatigue. *J Orthop Res*. 1998;16(3):322-329.
35. Hodgskinson R, Currey JD. Young's modulus, density and material properties in cancellous bone over a large density range. *J Mater Sci Mater Med*. 1992;3(5):377-381.
36. Hernandez CJ, Lambers FM, Widjaja J, Chapa C, Rimnac CM. Quantitative relationships between microdamage and cancellous bone strength and stiffness. *Bone*. 2014;66:205-213. doi:10.1016/j.bone.2014.05.023
37. Donnelly E, Boskey AL, Baker SP, van der Meulen MCH. Effects of tissue age on bone tissue material composition and nanomechanical properties in the rat cortex. *J Biomed Mater Res A*. 2009;92(3):1048-1056. https://onlinelibrary.wiley.com/doi/10.1002/jbm.a.32442
38. Grynpas M. Age and disease-related changes in the mineral of bone. *Calcif Tissue Int*. 1993;53(1 Suppl):S57-S64.

SUPPORTING INFORMATION

Additional supporting information can be found online in the Supporting Information section at the end of this article.

How to cite this article: Shaffer SK, Garcia TC, Stover SM, Fyhrie DP. Exercise history predicts focal differences in bone volume fraction, mineral density and microdamage in the proximal sesamoid bones of Thoroughbred racehorses. *J Orthop Res*. 2022;40:2831-2842. doi:10.1002/jor.25312